JBC Papers in Press. Published on May 29, 2019 as Manuscript RA119.007743
The latest version is at http://www.jbc.org/cgi/doi/10.1074/jbc.RA119.007743

Defining α-synuclein species responsible for Parkinson disease phenotypes in mice

Jessica M. Froula[1,*], Marta Castellana-Cruz[3,*], Nadia M. Anabtawi[1], José D. Camino[2], Serene W. Chen[3], Drake R. Thrasher[1], Jennifer Freire[1], Allen A. Yazdi[1], Sheila Fleming[4], Christopher M. Dobson[3], Janet R. Kumita[3], Nunilo Cremades[2,#], and Laura A. Volpicelli-Daley[1,#]

From the[1]Department of Neurology, Center for Neurodegeneration and Experimental Therapeutics; University of Alabama at Birmingham, Birmingham, AL, 35294 USA; [2]Institute for Biocomputation and Physics of Complex Systems (BIFI)-Joint Unit BIFI-IQFR (CSIC), University of Zaragoza, Zaragoza 50018, Spain; [3]Centre for Misfolding Diseases, Department of Chemistry, University of Cambridge, Cambridge CB2 1EW, United Kingdom; [4]Department of Pharmaceutical Sciences, Northeast Ohio Medical University, OH, USA

Running title: *α-synuclein conformers responsible for PD phenotypes*

[*]These authors contributed equally to this work.

[#]To whom correspondence should be addressed: Laura A. Volpicelli-Daley: Department of Neurology, Center for Neurodegeneration and Experimental Therapeutics; University of Alabama at Birmingham, Birmingham, AL, 35294; USA; lvolpicellidaley@uabmc.edu; Tel.(205)996-7695; Nunilo Cremades: Institute for Biocomputation and Physics of Complex Systems (BIFI)-Joint Unit BIFI-IQFR (CSIC), University of Zaragoza, Zaragoza 50018, Spain. ncc@unizar.es; Tel.(+34)876555415.

Keywords: alpha-synuclein (α-synuclein), amyloid, fibril, Lewy body, oligomer, Parkinson disease, protein aggregation, neurodegeneration, cytotoxicity, motor behavior defect

Abstract

Parkinson disease (PD) is a neurodegenerative disorder characterized by fibrillar neuronal inclusions composed of aggregated α-synuclein. These inclusions are associated with behavioral and pathological PD phenotypes. One strategy for therapeutic interventions is to prevent the formation of these inclusions in order to halt disease progression. α-Synuclein exists in multiple structural forms, including disordered, non-amyloid oligomers, ordered amyloid oligomers, and fibrils. It is critical to understand which conformers contribute to specific PD phenotypes. Here, we utilized a mouse model to explore the pathological effects of stable amyloid β-sheet oligomers compared with those of fibrillar α-synuclein. We biophysically characterized these species with transmission EM, atomic-force microscopy, CD spectroscopy, FTIR spectroscopy, analytical ultracentrifugation, and thioflavin T assays. We then injected these different α-synuclein forms into the mouse striatum to determine their ability to induce PD-related phenotypes. We found that β-sheet oligomers produce a small but significant loss of dopamine neurons in the substantia nigra pars compacta (SNc). Injection of small β-sheet fibril fragments, however, produced the most robust phenotypes, including reduction of striatal dopamine terminals, SNc loss of dopamine neurons, and motor behavior defects. We conclude that although the β-sheet oligomers cause some toxicity, the potent effects of the short fibrillar fragments can be attributed to their ability to recruit monomeric α-synuclein and spread *in vivo* and hence contribute to the development of PD-like phenotypes. These results suggest that strategies to reduce the formation and propagation of β-sheet fibrillar species could be an important route for therapeutic intervention in PD and related disorders.

Multiple neurodegenerative diseases are characterized by amyloid inclusions that are formed by the assembly of monomeric proteins into oligomeric intermediates that then grow to form protofilaments, and eventually fibrils (1). In Parkinson disease (PD), these inclusions are referred to as Lewy bodies and Lewy neurites and

are composed primarily of α-synuclein (2), but also include other proteins such as p62 and ubiquitin (3). They develop from the nucleated polymerization of endogenous α-synuclein that is then thought to spread within neurons and to propagate to interconnected neuronal networks in a spatially and temporally predictable manner (4,5). The role of α-syn in neurodegeneration and in generating symptoms in PD is not yet completely clear and is an area of active research. It is important to note that neurodegeneration is likely to be caused by a combination of factors in addition to α-synuclein inclusion formation such as impaired proteostasis, mitochondrial dysfunction, and activation of the inflammatory. On the basis of data that support the cell-to-cell spreading of α-synuclein aggregates, however, therapeutic strategies such as immunotherapy are in development in the hope of blocking the invasion of pathogenic α-synuclein species into additional brain regions and hence slowing the progression of PD (6).

Preventing the progression of α-synuclein inclusion formation, however, requires precise definitions of the species that are more highly toxic, and those that are capable of promoting the formation of new aggregates by recruiting endogenous monomeric α-synuclein. Assemblies of structurally diverse oligomers and fibrils have varying degrees of pathogenicity (7-9). In a cellular environment, monomeric α-synuclein interacts with membranes, and adopts an α-helical, tetrameric conformation (10-12). Monomeric α-synuclein can also assemble into fibrils in an array of heterogeneous oligomeric species that are often transient in nature. Recently, methods have been developed to produce and stabilize oligomers of α-synuclein (7,13), enabling these to be extensively characterized. One particularly well defined type of α-synuclein oligomeric species is composed of approximately 15-30 protein molecules, adopts a spherical appearance, and contains a rudimentary β-sheet structural core with very limited capability of binding the amyloid-specific dye thioflavin T (ThioT) and of elongating and recruiting new α-synuclein molecules. Addition of these oligomers to cells in culture disrupts membranes, generates reactive oxygen species, increases cytosolic calcium, and increases cell death (7,13,14). In contrast, the typical fibrillar forms of α-synuclein show the general amyloid features, including ability to bind ThioT, the presence of a cross-β core structure and an elongated filamentous morphology of 10-15 nm of diameter. Exposure of neurons to extracellular α-synuclein fibrils induces intracellular endogenous α-synuclein to form inclusions that are morphologically and biochemically similar to those found in diseased brains; they form dense Lewy body-like aggregates in the soma, thread-like Lewy-neurites in the neuropil, are insoluble in nonionic detergents, are primarily composed of fibrillar aggregates, and are phosphorylated, ubiquitinated, and proteinase K resistant (4,5,15,16). Inclusion formation leads to loss of dopaminergic neurons in the SNc with associated motor dysfunctional phenotypes, recapitulating the core features of PD. It has been shown that extensive sonication of α-synuclein fibrils increases the abundance of inclusions (17,18). Such fragmentation, however, can generate a heterogeneous ensemble of species, including oligomers as well as short and long fibrillar fragments, which likely contributes to the current variability of observed phenotypes in the pre-formed fibril (PFF) mouse model (19). More precise biophysical characterization combined with *in vivo* experiments is required to define which species contribute more strongly to the neuropathological and neurodegenerative phenotypes.

Here, we produce, isolate, and define reproducible conformers of mouse α-synuclein and monitor the neuropathological and neurodegenerative outcomes in mice injected with of different well-defined forms of the protein, namely monomers, stable kinetically-trapped β-sheet oligomers and fibril fragments. Unilateral injection of the β-sheet oligomers causes a slight, but significant loss of dopamine neurons in the SNc, but does not induce inclusion formation or produce defects in motor behavior; these findings can be attributable to the inability of these oligomers to grow by addition of the monomeric protein. The injections of preparations of short fibrils (70 nm), however, results in the formation of inclusions, the loss of dopamine terminals in the striatum, dopaminergic neurons in the SNc, and motor behavior defects.

Results

Biophysical and morphological characterization of α-synuclein conformers

In order to determine the capacity of different structural forms of α-synuclein in the mouse brain to induce PD-related phenotypes, we used recombinant mouse α-synuclein protein for the preparations of the different forms given the lower efficiency of seeding when using cross-species (i.e., human) α-synuclein forms ((20); see Figure 3). We first characterized the stability and structural features of oligomers and fibrils. α-Synuclein fibrils were generated by shaking monomeric α-synuclein for seven days at 37°C, and the resulting structures showed by transmission electron microscopy (TEM) and atomic force microscopy (AFM) indicated a long, filamentous structure as observed previously ("F-Long, F-L") with an average length of 266 ± 0.5 nm (Figure 1A-D). Shorter fibrils were then generated by sonication reducing the average length to 120 ± 4.0 nm; these fragments still, however, varied in length from 40-225 nm ("F-Mix, F-M") (Figure 1E-H). Samples enriched in shorter fragments were generated by passing the solution of F-M through a 0.22 μm filter (21,22), resulting in an average length of 70 ± 3.3 nm and a more homogenous distribution of 40-125 nm ("F-short, "F-S) (Figure 1I-L). Stabilized oligomeric species were generated using the procedure described previously for the human variant of the protein (7,14); these oligomers were observed in TEM and AFM images to have a spherical morphology that was similar to that observed for oligomers generated by human α-synuclein. Their size was more uniform than that of the fibrillar samples, with an average length of 54 ± 0.7 nm and a range of 40-70 nm (Figure 1M-P). To confirm that the procedures used to generate the oligomers and fibrils did not cause degradation of α-synuclein, oligomer, F-L, F-M, and F-S were incubated with urea to dissociate the fibrils and oligomers into monomers. α-Synuclein was identified using SDS-PAGE and bands were visualized using either "instant blue" or silver stain. Protein remains unaltered in all the protein samples, except for some minor monomer degradation occurred in the oligomeric samples with minimal consequences for the study (Supplemental Figure 1).

Indeed, the stable, purified oligomers generated by mouse α-synuclein show identical morphological and structural features as the previously reported oligomers of human α-synuclein (Figure 2A)(7). As previously shown for human oligomers, analytical ultracentrifugation (AUC) revealed that mouse oligomers showed two main distributions: one centered at 10S corresponding to a population of oligomers composed of an average of 18 α-synuclein molecules (260 kDa) and the other at 15 S, corresponding to oligomers composed of an average of 29 α-synuclein molecules (420 kDa) (Figure 2A), and similar to the size distribution of human oligomers. Also similar to the previously characterized human oligomers, mouse oligomers showed an intermediate structure between the disordered monomer and the β-sheet rich amyloid fibrils, with an average of 30% of β-sheet structure (F-L, F-M and F-S show ~ 60-65%) according to Fourier transform infrared (FTIR) and far-UV circular dichroism (CD) spectroscopy analysis (7,13) (Figure 2B,C). They also showed a marginal ability to bind ThioT molecules (Figure 2D), unlike F-L, F-M and F-S, which show similar ThioT binding. In addition, the FTIR data also showed a marked difference between the oligomers and the fibrils; while the spectra of the fibrils contain an absorbance peak at 1,620 cm^{-1} and no absorbance peak at 1695 cm^{-1}, characteristic of a parallel β-sheet configuration, the spectra of the oligomers clearly show both peaks demonstrating an antiparallel β-sheet arrangement. An antiparallel conformation for stabilized oligomers and parallel conformation for fibrils has previously been observed for human α-synuclein, and other amyloidogenic proteins and peptides such as amyloid-β (23,24), and the acquisition of the antiparallel β-sheet arrangement has been associated with a lower structural stability and a significantly reduced efficiency in elongation and seeding (7,25). Indeed, the stable oligomeric species (O) of α-synuclein appear to be trapped species that need to dissociate and reassemble into species with parallel β-sheet structure to readily assemble into fibrils. Antibodies have been generated which recognize toxic conformations of proteins implicated in neurodegeneration (26,27). The A11 antibodies selectively recognize potentially toxic conformations of proteins implicated in neurodegeneration, particularly pre-fibrillar oligomers, whereas OC recognizes fibrils. Dot-blots using these antibodies showed that as

expected, OC recognized FL, FM and FS. A11 recognized the oligomer preparation but also recognized the sonicated fibrils. A11, however, did not recognize the long fibrils (Supplemental Figure 2). These data indicate that the process of fragmenting longer fibrils can produce toxic oligomers as previously shown (13).

Seeding efficiency of fibrils and oligomers in vitro and in neurons

We first wanted to assess the degree of compatibility between human and mouse α-synuclein in *in vitro* seeding reactions (Figure 3A). Mouse and human fibrils (5μM) were combined with 100μM mouse α-synuclein monomer, and the formation of ThioT positive amyloid fibrils was measured over time. Mouse fibrils seeded the formation of ThioT-positive amyloid fibrils from mouse α-synuclein monomer more rapidly than human fibrils as previously shown (20). Interestingly, the initial rate of seeding using fibrils and monomers of human α-synuclein protein was slower than that observed for mouse α-synuclein and was significantly slower when mouse α-synuclein fibrils were used to seed solutions of human α-synuclein monomers. Thus, the seeding efficiency was found to be higher when the species of α-synuclein seeds matches that of the free monomers; therefore, in the *in vivo* seeding studies that involve endogenous expression of mouse α-synuclein, it is recommended to use fibrillar seeds generated from mouse α-synuclein.

Using the mouse protein, the ability of the oligomers and the different sizes of fibrils to seed formation of ThioT-positive amyloid fibrils was also determined (Figure 3B). Seeding with the oligomers was highly inefficient and produced negligible fibril formation over time, a finding consistent with previous data for the human protein showing that these oligomers are trapped in a conformation distinct from that of the fibrillar species that is unable to efficiently elongate (7). In contrast, all the fibrillar samples used in this study were highly efficient in the seeding reactions.

To examine the ability of different α-synuclein fibrils to seed inclusion formation in neurons, 0.05 μM concentrations of monomeric, O, F-L, F-M or F-S were added to wild type primary hippocampal neurons and the abundance of phosphorylated α-synuclein, a marker of pathological α-synuclein inclusion formation in cells, was measured (28) (Figure 3C,D). Neither monomeric nor oligomeric α-synuclein was found to produce p-α-synuclein inclusions, a result consistent with the finding that these forms of α-synuclein were not able to seed fibril formation *in vitro*. Immunofluorescence appeared diffuse and faint in experiments with both forms of α-synuclein. F-M and F-S produced similar quantities of inclusions, the majority of which appeared as bright and thread-like structures similar to Lewy-neurites found in synucleinopathies brains. In contrast, a small quantity of p-α-synuclein was visible in neurons exposed to the long fibrils; significantly lower compared to the levels observed in neurons exposed to fragmented fibrils (Figure 3C,D). To determine if fibrils are more efficient at inducing α-synuclein inclusion formation because they are more efficiently internalized than oligomers, an internalization assay using α-synuclein labeled with Alexa488 was performed (29). This assay utilizes trypan blue to quench the fluorescence of extracellular α-synuclein conformers to distinguish extracellular from intracellular α-synuclein. In addition, when trypan blue binds to proteins on the membrane surface, it fluoresces when excited at 560nm, allowing visualization of soma and neurites. Both short Alexa488 labelled α-synuclein fibrils (F-S) and oligomers (O) were internalized, while unsonicated fibrils showed minimal internalization as demonstrated previously (29) (Figure 3E). Surprisingly, oligomers showed significantly increased internalization compared to fibrils, indicating that efficiency of fibril uptake does not account for robust inclusion formation. Table 1 summarizes the structural and morphological features of all the α-synuclein species used in this study.

Formation of inclusions in the brain by fibrils and oligomers

To determine the extent to which the oligomers and the different lengths of fibrils seed the formation of α-synuclein inclusions in the brain, mice received unilateral striatal injections of each species with the mass concentrations in the samples measured immediately after injection. Monomeric α-synuclein was also injected as a control. In the case of the oligomeric samples, the concentration of α-synuclein was determined by

absorbance at 280 nm (the extinction coefficient used was 8278 $M^{-1}cm^{-1}$ for oligomers); the fibrillar samples were first dissociated into monomeric units using guanidinium hydrochloride and the concentration of protein in the sample was then determined (the extinction coefficient used was 7450 $M^{-1}cm^{-1}$). The concentration of the oligomers was determined to be 300 μM, and that of F-L, F-M, and F-S to be 150 μM, although the fibrils were initially prepared using 300 μM α-synuclein. Since this study was initiated, we published a recommendation that fibrils should be freshly made before injections, rather being frozen and that the concentration of fibrils should be measured immediately before injection (19). Thus, the concentration of oligomers injected was twice that of the fibrils in terms of monomer equivalents.

The mice were perfused 3 months after injection of the α-synuclein species. Immunohistochemistry was performed using an antibody specific for α-synuclein phosphorylated at serine-129, one of the post-translational modifications of α-synuclein in Lewy neurites and Lewy bodies in synucleinopathy brains (28). In synucleinopathy models, there is very little pSer129-α-synuclein in neurons from control wild type mice. However, exposure of neurons to fibrils, produces α-synuclein abundant inclusions that are highly phosphorylated (5). These fibril-induced inclusions have also been shown in previous studies to be ubiquitin and p62 positive, and are insoluble in detergent (5,16,30-32). Importantly, when neurons from α-synuclein knockout mice are exposed to fibrils, the neurons show minimal pSer129-α-synuclein immunoreactivity (4). In both monomer and oligomer injected mice (Figure 4A) immunoreactivity for p-α–synuclein appeared to be diffuse in the cytosol, possibly representing a pool of monomeric α–synuclein protein targeted for degradation (33). Unilateral striatal injections of F-L, F-M, and F-S all resulted in the formation of p-α-synuclein positive inclusions that produced more intense signals compared to oligomer injected mice. The inclusions appeared as Lewy-neurite like threads in the neuropil and skein-like inclusions in the soma. The abundance of neurons with inclusions in the soma was measured using a semi-quantitative rating scale (Supplemental Figure 3) and the average level within the animals in each group was calculated. Table 2 shows the list of the brain areas containing inclusions along with a ranking based on the quantification process in the different brain areas. The brain areas with the most abundant inclusions included the cortex, amygdala and striatum. Except for the SNc, which only showed inclusions on the side ipsilateral to the injection, all the brain areas investigated showed bilateral inclusions after unilateral injections of α-synuclein species in the striatum, although the ipsilateral side consistently showed more inclusions than the contralateral side (Figure 4C). The fragmented fibrils (F-M, F-S) produced significantly more inclusions than non-fragmented fibrils (F-L), although there were no significant differences in the abundance of inclusions between F-M and F-S injected mice (Figure 3).

Appearance of p-α-synuclein inclusions in different brain regions at different time points following injections of fibrillar species

The most abundant inclusions appear in the cortex, amygdala, and SNc. These brain regions all project to the striatum (34), suggesting that the aggregates are internalized into the axon terminals, and the resulting inclusions spread within the neuron to the soma. This is consistent with findings that after addition of fibrils to neurons of nontransgenic mice endogenously expressing α-synuclein, inclusions appear first in axons and then at later time points in the soma (4), and is also consistent with the highest concentration of α-synuclein being at the presynaptic terminals (35). To confirm the observation that inclusions appear in brain nuclei that project to the striatum, we co-injected the fibrillar samples with retrotracer beads into the right dorsal-lateral striatum. Neither the retrotracer beads nor p-α-synuclein-positive inclusions had appeared in the SNc (Figure 5A) or amygdala one week after injections. In the cortex, however, small fluorescent p-α-synuclein puncta that were colocalized with retrotracer beads were visible. Two weeks after injection, however, p-α-synuclein-positive inclusions were visible in the SNc, cortex and amygdala in the same area as the retrotracer beads. By four weeks after injection, p-α-synuclein-positive inclusions were abundant in all three brain regions. These data show that the formation of p-α-synuclein-positive inclusions after injection of fibrils is not apparent until about one week after injections and that the cortex is the first area affected.

Loss of dopamine terminals in the striatum and dopamine neurons in the SNc

Unilateral injection of sonicated fibrils into the striatum was previously shown to produce a significant, approximately 35%, loss of dopaminergic neurons in the SNc relative to mice injected with saline solution (5). The loss occurred 6 months following injection of fibrils, whereas there were no statistically significant differences in the numbers of tyrosine hydroxylase (TH)-positive dopamine neurons 3 months after injection. We used, here, unbiased stereology to quantify the numbers of TH-positive neurons in the ipsilateral and contralateral SNc of mice unilaterally injected with the different α-synuclein species. Three months after injection, only F-S produced a significant, approximately 30% loss of dopaminergic neurons compared to monomer injected mice in the ipsilateral SNc (Figure 6). The number of dopaminergic neurons on the side ipsilateral to the injection site were significantly reduced relative to the non-injected side (Figure 6B). Oligomers produced a significant reduction in the number of neurons on the side ipsilateral to the injection site relative to the non-injected side. To determine if dopamine neurons are dying in mice injected with α-synuclein species, or if TH levels are simply being downregulated, double labeling immunofluorescence measurements for TH and NeuN (Supplemental Figure 4) was performed in the SNc. Compared to mice that received unilateral injections of monomeric α-synuclein, there was a slight, but not statistically significant, reduction in the number of NeuN positive neurons in the mice that received unilateral injections of F-S. The TH-immunofluorescence in the F-S and O-injected mice appeared beaded compared to monomer injected mice, suggestive of dying neurons. However, there were also TH-positive neurons that appeared healthy. These findings suggest the existence TH-positive-dopaminergic and non-dopaminergic neuron subtypes in the SNc that resist toxic α-synuclein fibrils.

The loss of dopamine terminals from the striatum was measured by immunofluorescence detection of the dopamine transporter (DAT) (Figure 6 C,D). Mice injected with both F-M and F-S showed a significant, approximately 30%, reduction in DAT-positive dopamine terminals relative to monomer injected mice. However, only F-M injected mice showed a statistically significant loss of TH-positive axons in the SNc (Supplemental Figure 5). The difference between DAT and TH labeling in the striatum could simply result from technical differences in immunofluorescence labeling, or differences between vesicular localized DAT vs. cytosolic localized TH. Alternatively, the possible interaction between α-synuclein aggregates and DAT may alter the trafficking and localization of this transporter, which could potentially be an interesting line of investigation for the future. In addition, unlike the unilateral loss of dopamine neurons in the SNc, the loss of dopamine terminals in the striatum was bilateral. Thus, smaller fibrils of α-synuclein cause a loss of dopamine neurons and dopamine terminals at 3 months following injections.

Motor behavior defects caused by fibrils and oligomers

We next determined if injection of fibrils and the consequent loss of dopaminergic neurons and terminals were associated with defects in motor behavior. After 3 months, only mice that received unilateral injections of F-S showed a significant increase relative to untreated mice in the time needed to descend a pole, a well-established test for "bradykinesia" (36) (Figure 7). Using the cage hang test, a test of motor strength, it was found that only F-S injected mice also dropped from the lid of a cage in consistently shorter times compared to control mice, also indicative of motor defects (5). There were no significant differences among any of the groups of treated mice in an open field test for time spent in the center of the field (a measure of "anxiety) or in the speed of movement. A cylinder test modified specifically for mice (37) also showed no differences among the groups in the average numbers of hind limb steps or rears. Injections of short fragments of fibrils, therefore, show much greater defects in behavioral tests of bradykinesia and motor strength compared to much larger fibrils and toxic but propagation-deficient oligomers.

Discussion

Designing therapeutic strategies to halt the progression and spread of synucleinopathies such as PD requires characterization of the specific

forms of α-synuclein that are responsible for given phenotypes, including the formation of inclusions in multiple brain areas, the loss of dopamine terminals, the reduction in the numbers of neurons in the SNc, and the loss of normal motor behavior. In the present study, we have used a combination of biophysical, biochemical and behavioral assays to demonstrate that small aggregates composed primarily of small fragments of α-synuclein fibrils are able to induce typical features of PD when injected into the brains of healthy mice. Such aggregates are able to grow and recruit endogenous monomeric α-synuclein, suggesting that these species are important agents for the spreading of toxicity and disease. By contrast, stable oligomeric aggregates of α-synuclein, which do not undergo elongation, were unable to induce the formation of inclusions by endogenous α-synuclein, to cause loss of dopamine terminals in the striatum, to cause loss of dopamine neurons in the SNc, or to cause deficiencies in motor behavior. The oligomers, however, caused a significant loss of dopamine neurons in the SNc on the side ipsilateral to the injection compared to the contralateral side, a finding consistent with their established cytotoxic nature but lack of seeding potency (7,14,38,39). Considering all the present results together, we demonstrate that other properties, in addition to toxicity, such as the ability of aggregates to seed the formation of new aggregates and to spread between cells, are important for the induction of PD phenotypes in an animal model, and that the α-synuclein species that are most efficient in spreading pathology are small fibrillar aggregates, and particularly fibrillar oligomers with high seeding efficiency. Indeed our results suggest that the ability of aggregated species to recruit monomeric protein molecules and to generate new toxic aggregates is a more important feature than the inherent toxicity of the injected species for the development of PD-related phenotypes (i.e. highly toxic, seeding-deficient oligomers vs. less toxic and seeding competent small fibrils). In addition, our results suggest that the major disease spreading agents consist of seeding-efficient α-synuclein small fibrillar aggregates rather than the possible specific conformers generated from the toxic cascade of events induced by the toxic aggregates and that could be transferred from damaged to healthy cells. Finally, given the potential highly toxic and seeding-competent nature of the fibrillar oligomers generated during the aggregation reaction, in contrast to the seeding-deficient features of the kinetically trapped oligomers used in this study, as well as their high efficiency in enabling cell internalization compared to the fibrillar species, we hypothesize that these species are also likely to be important players in the development and spreading of disease. Indeed, we have recently observed that the interaction of extracellular short fibrillar species with cells results in the generation of on-pathway oligomers that are readily internalized (manuscript under review) and that could therefore efficiently seed the intracellular formation of new toxic aggregates. Overall, our results highlight the importance of fibrillar aggregates of α-synuclein in the induction of PD-related phenotypes. Future studies to examine the mechanisms by which larger inclusions can fragment within the cell to become new and efficient nuclei for the propagation of α-synuclein inclusions and disease phenotypes will be of great interest, including disaggregation by chaperones or lysosomal proteases (40).

Our results suggest that inhibiting the accumulation of small fibrillar α-synuclein fragments generated either during the process of protein aggregation or by the fragmentation or disaggregation of longer fibrils, have the potential to be a therapeutic strategy against PD progression. Indeed, immunotherapy using antibodies raised against α-synuclein are in phase II clinical trials (6). However, antibodies that are not selective for fibrillar α-synuclein also reduce the total concentration of α-synuclein, and may have deleterious effects because decreasing levels of α-synuclein impairs dopamine transmission (41,42). Antibodies that selectively target fibrillar aggregates and reduce their ability to spread from cell-to-cell could therefore reduce the rate of disease propagation. One example is BIIB054 which selectively binds fibrillar α-synuclein (43), and in mouse models of PD, intraperitoneal injections of this antibody inhibited inclusion formation, dopamine neuron loss, and defects in motor behavior.

It has been shown that formation of α-synuclein oligomers *in vivo* by expression of human α-synuclein pathological variants using lentivirus induces loss of dopamine neurons (44). The oligomers used in our present study have anti-

parallel β-sheet structure, while the fibrillar structures are parallel, and so they are unable to elongate as they are kinetically trapped. It is likely that oligomers containing a parallel ß-sheet structure are transient species involved in the formation of fibrils and are therefore able to elongate and proliferate. In addition, it is also likely that a range of different types of oligomeric species exist *in vivo*, including species bearing post-translational modifications, which are likely to share with the fibrillar species the ability to disrupt membranes and perturb other cellular processes such mitochondrial function (45,46).

Overall, our data highlight the importance of precise biophysical definitions of the aggregated forms of α-synuclein that are responsible for the major events of dysfunction related to PD. In this study, injection of the small fibrillar fragments (~70 nm in length) produced p-α-synuclein inclusions, neuronal loss and motor dysfunction. The fibril preparation, similar to that used in previous studies (5,30) containing longer fragments (40-225 nm) produced p-α-synuclein inclusions, but did not cause significant dopamine neuron loss or behavioral phenotypes at three months following injections. This result indicates that fibril preparations enriched for small fragments will produce the most robust phenotypes. Although the fibril model is becoming widely accepted for reproducing PD-like pathology, variability has been reported in obtaining phenotypes which could be caused by heterogeneous fibril preparations with a wide range of fibril sizes.

Although the length of fragments does not substantially influence the seeding of fibril formation *in vitro*, smaller fragments are required for seeding of α-synuclein pathology in neurons and in the brain. This is likely to be because the smaller fragments bind more efficiently to cell surface receptors such as Lag3, Na^+K^+ATPase and heparin sulfate proteoglycans, and only the smaller fragments can be internalized by endocytosis (47-49). Furthermore, smaller fragmented fibrils are the most likely species to be released from neurons and to propagate throughout the brain.

Our study adds to the results of earlier investigations that demonstrated that aggregates consisting solely of α-synuclein can generate PD phenotypes (5,16,30,31,50). However, in the future, it will be of great interest to characterize the structural properties of aggregates purified from diseased brains. Interestingly, brain extracts from patients with multiple system atrophy (MSA) have been reported to be more effective than those from PD brains at inducing α-synuclein inclusion formation and disease spreading when injected into experimental animals (51,52). α-Synuclein species involved in Lewy Body disease may bind receptors in the cortex and limbic regions more readily than do species involved in PD, which may bind more efficiently to receptors in the SNc. Future studies are required to determine how different aggregates contribute to specific disease phenotypes. Overall, our findings indicate that small fibrillar aggregates of α-synuclein are necessary for inducing pathology and spreading, and suggest that therapeutics should aim to reduce formation and accumulation of such species.

Experimental Procedures

Animals. All animal protocols were performed at AAALAC accredited sites and approved by the University of Alabama at Birmingham Institutional Animal Care and Use Committee. C57BL/6 J male mice were obtained from Jackson laboratories and housed in groups of no more than five animals per cage. Food and water were accessible 24 h, and animals were kept on a 12 h light/dark cycle.

Preparation of α-synuclein species. α-synuclein monomer was purified according to previously published protocols (53). The presence of endotoxin was detected using the Pierce LAL chromogenic endotoxin quantitation kit and cleaned using Pierce high capacity endotoxin removal spin columns. Endotoxin levels were measured to be less than 0.0113 ng/mL. α-Synuclein fibrils were prepared as previously published(53). Before surgeries, fibrils were sonicated using a 1/8" probe tip sonicator, (Fisher cat no. FB120110) at 30% power, for 30 sec total, 1 sec on, 1 sec off. Short fibrils were isolated using an EMD Millipore Millex 0.22 uM filter unit. Immediately before injections of monomeric α-synuclein, α-synuclein protein was spun at 20,000*g* at 4ºC. β-sheet kinetically trapped α-synuclein oligomers were freshly prepared as described previously (7,13,14). Briefly, 6 mg of lyophilized protein was resuspended in PBS buffer at a pH of 7.4 and at a concentration of 12 $mg.ml^-$

[1]. The solution was filtered through a 0.22 μm cutoff filter and subsequently incubated at 37 °C for 24 h in stationary mode and without agitation. Small numbers of fibrillar species formed during the incubation were removed by ultracentrifugation for 1 h at 90,000 rpm (using a TLA-120.2 Beckman rotor; 288,000g). The excess of monomers and small oligomers in the sample was then removed by means of several filtration steps using 100 kDa cutoff membranes, which resulted in the enrichment and concentration of the oligomeric α-synuclein species. The oligomers prepared in this manner have been found to be stable for many days (7). They were shipped from Cambridge the same day of preparation and injected the day of receipt (one/two days after preparation) to ensure a stable, characterized conformation.

Biophysical characterization of α-synuclein conformers. A comparative morphological and structural analysis of the different conformers has been performed using a variety of complementary biophysical techniques, and a detailed structural analysis has recently been carried out with oligomers of human α-synuclein using both cryo-EM and solution and solid-state NMR spectroscopy (7,14). TEM images were obtained using a Philips CEM100 transmission electron microscope (CAIC, University of Cambridge UK). The samples were applied to Formvar carbon coated nickel grids, washed with ddH2O and negatively stained with 2% (w/v) uranyl acetate. AFM images were acquired using tapping mode in a Multimode 8 atomic force microscope (Bruker, Massachusetts, USA). The different α-synuclein species (0.1-1 μM, 10 μL) were applied onto a layer of freshly cleaved mica and allowed to air-dry. The samples were washed with water to remove any salts and dried again before imaging. Images were processed with Gwyddion open source software (http://www.gwyddion.net). Sedimentation velocity measurements using AUC were carried out at 20 °C at 38,000 to 43,000 rpm (106,750 to 136,680 × g) by using a Beckman-Coulter Optima XL-I analytical ultracentrifuge with an An-50 Ti rotor (Beckman-Coulter, Brea, CA, USA). The sedimentation coefficient distributions, corrected to standard conditions by using the SEDNTERP program (54), were calculated via least-squares boundary modeling of sedimentation velocity data using the c(s) and lsg*(s) methods, as implemented in the SEDFIT program (www.analyticalultracentrifugation.com). FTIR spectra of the different α-synuclein species (100-400 μM) were acquired in PBS and analyzed in a Bruker BioATRCell II using a Bruker Equinox 55 FTIR spectrophotometer (Bruker Optics Limited, UK) equipped with a liquid nitrogen cooled mercury cadmium telluride (MCT) detector and a silicon internal reflection element (IRE). For each spectrum, 256 interferograms were recorded at 2 cm^{-1} resolution. Data processing of the amide I region (1720-1580 cm^{-1}) was performed with the Opus software package (Bruker Optics Limited, UK) and consisted of a background subtraction of the buffer spectrum, atmospheric compensation and baseline subtraction. All absorbance spectra were normalized for comparison. Far-UV CD spectra of the different α-synuclein species were acquired at 20 °C between 200 nm and 250 nm, using a scan speed of 50 nm min^{-1} and a bandwidth of 1 nm. 10 accumulations were recorded for each sample, using a 1 mm path length cuvette and a J-810 Jasco spectropolarimeter (Tokyo, Japan), equipped with a thermostated cell holder. The signal was converted to mean residue ellipticity (M.R.E.). ThioT fluorescence measurements were performed in a 2 mm x 10 mm path length cuvette, using a Varian Cary Eclipse fluorimeter (Palo Alto, CA, USA) in a temperature-controlled cell holder, exciting the sample at 446 nm and recording the emission fluorescence spectrum between 460 to 600 nm (5nm slitwidths). Each protein species (10 μM) was incubated with ThioT (50 μM, 416nm = 26620 M^{-1} cm^{-1}) for 30 min before performing the measurement. For the seeding experiments, 10μM of each protein species (or 5μM in the case of the cross-seeding experiments) were added to a solution of 100 μM α-synuclein monomer, 50μM ThioT and 0.02% (w/v) sodium azide. The ThioT fluorescence was recorded in a BMG Fluostar Optima (BMG LABTECH, Aylesbury, Bucks, UK) using a excitation filter of 440 nm an and emission filter of 480 nm, at a constant temperature of 37 °C.

Primary neurons were plated at 100,000 neurons per well in a 24 well tray onto poly-d-lysine coated coverslips and maintained in Neurobasal media, Glutamax, and B27 as previously described. The different conformers of α-synuclein were added to neurons at seven days *in vitro* at a

final concentration of 70 nM. Neurons were fixed 7 days later and immunofluorescence to p-α-synuclein (Abcam) and tau (Dako) was performed as previously described (4).

Internalization assay was essentially performed as described (29) with some modifications. We thus generated Alexa 488 labeled fibrils and oligomers using the α-synuclein mutant E122C in order to incorporate the fluorophore at the upstream position of the recognized C-terminal truncation sites. E122C α-synuclein was purified and labeled using Life technologies Alexa Fluor 488 C_5 maleimide. The labelled protein was purified from free dye using a P10 desalting column and a Sephadex G25 matrix. To perform the internalization experiments, primary neurons were incubated for 30 minutes in cold PBS containing α-synuclein-Alexa488 fibrils or oligomers (final concentration 70 nM) to allow the species to bind the plasma membrane. The neurons were then transferred to 37°C to allow internalization. Extracellular α-syn-Alexa488 fibrils were quenched with freshly made trypan blue, final concentration 1 mM in PBS. Images were captured using a Zeiss Axio Observer Z1 with Colibri LED illumination. The excitation/emission was 470/550 nm for the fibrils and 560/630 nm for trypan blue. The average intensity of each frame captured was quantified using Fiji and normalized to the fluorescence signal from trypan blue bound to the neuronal membrane.

Surgeries. Surgeries were performed using C57BL6/J mice aged two to four months using a digital stereotaxic frame (David Kopf). For the duration of surgery, mice were deeply anesthetized with vaporized isoflurane on a gas mask fitted to a digital stereotaxic frame. Mouse respiration was monitored throughout the procedure. Proteins for injection were drawn to a gas-tight syringe with a 26s gauge needle (Hamilton) and controlled by a digital pump. Two µL of protein were injected and subsequent withdrawal of needle occurred over the course of 12 min. Solutions were injected into the right dorsal striatum using the following coordinates: 0.2 mm anterior and 2.0 mm lateral to the Bregma, and 2.6 mm ventral relative to the skull. Scalp incisions were closed with EZ-Clips (FisherSci).

Immunohistochemistry and immunofluorescence. Mice injected with various α-syn conformations were anesthetized post injection with isofluorane and transcardially perfused with a saline solution (0.9% NaCl, 0.005% sodium nitroprusside, and 10 units/mL heparin sodium) followed by freshly prepared 4% paraformaldehyde (PFA) buffered in phosphate buffered saline (PBS). Brains were removed, postfixed for 24 h in 4% PFA and PBS solution, floated into 30% sucrose PBS solution for up to three days, frozen in methylbutane solution (−50 °C), and stored at −80 °C. Brain tissue was sectioned at 40 µM with a freezing microtome. Immunohistochemistry and immunofluorescence was performed as described previously (55). Antibodies included: p-α-synuclein (EP1536Y (Abcam)) (56), tyrosine hydroxylase (Abcam), dopamine transporter (a generous gift from Dr. Allan Levey, Emory University (57). For the DAT and TH immunofluorescence in the striatum, confocal images of coronal sections (Bregma: -0.5 mm anterior/posterior) were captured, and Image J was used to quantify the integrated intensity of the dorsal portion of the striatum.

Behavior Assays. All behavioral tests were performed with the help of our UAB Neuroscience Behavioral Core. Mice were acclimated to the test environment for at least 30 min prior to testing and were given at least a 1-day rest between each test. *Open Field Test* Each mouse was placed at the side of a 100 × 100 × 50 cm white Plexiglass open field. A computerized tracking system (Ethovision) recorded movement for 5 minutes from which we derived the following: the amount of time spent in the center of the test apparatus, and the velocity of movement. *Cylinder test* Mice were placed in a covered plexiglass cylinder with activity recorded for 5 min by Ethovision software on a camera positioned underneath the cylinder. An experimenter blinded to the treatment conditions scored each video. The following behaviors were scored: number of rears, front limb steps, hind limb steps, and total steps (37). *Pole Test* Mice were placed on top of a wooden pole (diameter 1 cm; height 50 cm) wrapped in chicken wire. Each subject completed 5 trials with a 1-minute rest between each trial. Time to turn with nose facing down and time to reach the bottom of the pole were recorded and combined to derive the total time to descend. If a mouse did not climb down the pole after 2 min, the trial time was not included in that animal's average total time to descend. *Cage Hang* Mice were placed on a cage

top elevated 50 cm above a cage filled with bedding. The cage lid was shaken slightly and flipped over to measure latency to fall over the course of 3 trials (> 1 min rest between each trial). A trial less than 10 seconds was performed again, and trials were concluded at 3 min if a mouse was still hanging.

Stereology Stereology was completed using an Olympus BX51 microscope and StereoInvestigator software (MBF Biosciences) using the UAB Neuroscience Molecular Detection and Stereology Core. Contours were drawn around 6-7 serial sections containing SNc. Unbiased stereological estimation of total TH-positive neurons in the SNc contralateral and ipsilateral to injection was performed using the Optical Fractionator probe by an investigator blinded to experimental conditions.

Statistical Analyses. Data were analyzed using GraphPad Prism. One-way or two-way ANOVA were performed. Outliers were identified using the ROUT method in Graphpad Prism. The only data in which 2 outliers were identified were in the cage hang motor test.

Acknowledgments. We would like to thank Andrew West for advice and suggestions on this work and Valentina Krendelchtchikova for help with purifying protein.

Conflict of interest The authors declare that they have no conflicts of interest with the contents of this article.

References

1. Cremades, N., and Dobson, C. M. (2018) The contribution of biophysical and structural studies of protein self-assembly to the design of therapeutic strategies for amyloid diseases. *Neurobiol Dis* **109**, 178-190
2. Spillantini, M. G., Schmidt, M. L., Lee, V. M., Trojanowski, J. Q., Jakes, R., and Goedert, M. (1997) Alpha-synuclein in Lewy bodies. *Nature* **388**, 839-840
3. Kuusisto, E., Parkkinen, L., and Alafuzoff, I. (2003) Morphogenesis of Lewy bodies: dissimilar incorporation of alpha-synuclein, ubiquitin, and p62. *J Neuropathol Exp Neurol* **62**, 1241-1253
4. Volpicelli-Daley, L. A., Luk, K. C., Patel, T. P., Tanik, S. A., Riddle, D. M., Stieber, A., Meaney, D. F., Trojanowski, J. Q., and Lee, V. M. (2011) Exogenous alpha-synuclein fibrils induce Lewy body pathology leading to synaptic dysfunction and neuron death. *Neuron* **72**, 57-71
5. Luk, K. C., Kehm, V., Carroll, J., Zhang, B., O'Brien, P., Trojanowski, J. Q., and Lee, V. M. (2012) Pathological alpha-synuclein transmission initiates Parkinson-like neurodegeneration in nontransgenic mice. *Science* **338**, 949-953
6. Volpicelli-Daley, L., and Brundin, P. (2018) Prion-like propagation of pathology in Parkinson disease. *Handbook of clinical neurology* **153**, 321-335
7. Chen, S. W., Drakulic, S., Deas, E., Ouberai, M., Aprile, F. A., Arranz, R., Ness, S., Roodveldt, C., Guilliams, T., De-Genst, E. J., Klenerman, D., Wood, N. W., Knowles, T. P., Alfonso, C., Rivas, G., Abramov, A. Y., Valpuesta, J. M., Dobson, C. M., and Cremades, N. (2015) Structural characterization of toxic oligomers that are kinetically trapped during alpha-synuclein fibril formation. *Proc Natl Acad Sci U S A* **112**, E1994-2003
8. Bousset, L., Pieri, L., Ruiz-Arlandis, G., Gath, J., Jensen, P. H., Habenstein, B., Madiona, K., Olieric, V., Bockmann, A., Meier, B. H., and Melki, R. (2013) Structural and functional characterization of two alpha-synuclein strains. *Nat Commun* **4**, 2575
9. Melki, R. (2018) How the shapes of seeds can influence pathology. *Neurobiol Dis* **109**, 201-208
10. Dettmer, U., Newman, A. J., Soldner, F., Luth, E. S., Kim, N. C., von Saucken, V. E., Sanderson, J. B., Jaenisch, R., Bartels, T., and Selkoe, D. (2015) Parkinson-causing alpha-synuclein missense mutations shift native tetramers to monomers as a mechanism for disease initiation. *Nat Commun* **6**, 7314
11. Burre, J., Sharma, M., and Sudhof, T. C. (2014) alpha-Synuclein assembles into higher-order multimers upon membrane binding to promote SNARE complex formation. *Proc Natl Acad Sci U S A* **111**, E4274-4283
12. Chandra, S., Chen, X., Rizo, J., Jahn, R., and Sudhof, T. C. (2003) A broken alpha -helix in folded alpha -Synuclein. *J Biol Chem* **278**, 15313-15318
13. Cremades, N., Cohen, S. I., Deas, E., Abramov, A. Y., Chen, A. Y., Orte, A., Sandal, M., Clarke, R. W., Dunne, P., Aprile, F. A., Bertoncini, C. W., Wood, N. W., Knowles, T. P., Dobson, C. M., and Klenerman, D. (2012) Direct observation of the interconversion of normal and toxic forms of alpha-synuclein. *Cell* **149**, 1048-1059
14. Fusco, G., Chen, S. W., Williamson, P. T. F., Cascella, R., Perni, M., Jarvis, J. A., Cecchi, C., Vendruscolo, M., Chiti, F., Cremades, N., Ying, L., Dobson, C. M., and De Simone, A. (2017) Structural basis of membrane disruption and cellular toxicity by alpha-synuclein oligomers. *Science* **358**, 1440-1443
15. Osterberg, V. R., Spinelli, K. J., Weston, L. J., Luk, K. C., Woltjer, R. L., and Unni, V. K. (2015) Progressive aggregation of alpha-synuclein and selective degeneration of lewy inclusion-bearing neurons in a mouse model of parkinsonism. *Cell Rep* **10**, 1252-1260
16. Masuda-Suzukake, M., Nonaka, T., Hosokawa, M., Kubo, M., Shimozawa, A., Akiyama, H., and Hasegawa, M. (2014) Pathological alpha-synuclein propagates through neural networks. *Acta neuropathologica communications* **2**, 88
17. Abdelmotilib, H., Maltbie, T., Delic, V., Liu, Z., Hu, X., Fraser, K. B., Moehle, M. S., Stoyka, L., Anabtawi, N., Krendelchtchikova, V., Volpicelli-Daley, L. A., and West, A. (2017) alpha-

Synuclein fibril-induced inclusion spread in rats and mice correlates with dopaminergic Neurodegeneration. *Neurobiol Dis* **105**, 84-98
18. Tarutani, A., Suzuki, G., Shimozawa, A., Nonaka, T., Akiyama, H., Hisanaga, S., and Hasegawa, M. (2016) The Effect of Fragmented Pathogenic alpha-Synuclein Seeds on Prion-like Propagation. *J Biol Chem* **291**, 18675-18688
19. Polinski, N. K., Volpicelli-Daley, L. A., Sortwell, C. E., Luk, K. C., Cremades, N., Gottler, L. M., Froula, J., Duffy, M. F., Lee, V. M., Martinez, T. N., and Dave, K. D. (2018) Best Practices for Generating and Using Alpha-Synuclein Pre-Formed Fibrils to Model Parkinson's Disease in Rodents. *J Parkinsons Dis*
20. Luk, K. C., Covell, D. J., Kehm, V. M., Zhang, B., Song, I. Y., Byrne, M. D., Pitkin, R. M., Decker, S. C., Trojanowski, J. Q., and Lee, V. M. (2016) Molecular and Biological Compatibility with Host Alpha-Synuclein Influences Fibril Pathogenicity. *Cell Rep* **16**, 3373-3387
21. Xu, G., Gonzales, V., and Borchelt, D. R. (2002) Rapid detection of protein aggregates in the brains of Alzheimer patients and transgenic mouse models of amyloidosis. *Alzheimer disease and associated disorders* **16**, 191-195
22. Chang, E., and Kuret, J. (2008) Detection and quantification of tau aggregation using a membrane filter assay. *Analytical biochemistry* **373**, 330-336
23. Celej, M. S., Sarroukh, R., Goormaghtigh, E., Fidelio, G. D., Ruysschaert, J. M., and Raussens, V. (2012) Toxic prefibrillar alpha-synuclein amyloid oligomers adopt a distinctive antiparallel beta-sheet structure. *The Biochemical journal* **443**, 719-726
24. Cerf, E., Sarroukh, R., Tamamizu-Kato, S., Breydo, L., Derclaye, S., Dufrene, Y. F., Narayanaswami, V., Goormaghtigh, E., Ruysschaert, J. M., and Raussens, V. (2009) Antiparallel beta-sheet: a signature structure of the oligomeric amyloid beta-peptide. *The Biochemical journal* **421**, 415-423
25. Qiang, W., Yau, W. M., Luo, Y., Mattson, M. P., and Tycko, R. (2012) Antiparallel beta-sheet architecture in Iowa-mutant beta-amyloid fibrils. *Proc Natl Acad Sci U S A* **109**, 4443-4448
26. Kayed, R., Canto, I., Breydo, L., Rasool, S., Lukacsovich, T., Wu, J., Albay, R., 3rd, Pensalfini, A., Yeung, S., Head, E., Marsh, J. L., and Glabe, C. (2010) Conformation dependent monoclonal antibodies distinguish different replicating strains or conformers of prefibrillar Abeta oligomers. *Mol Neurodegener* **5**, 57
27. Kayed, R., Head, E., Thompson, J. L., McIntire, T. M., Milton, S. C., Cotman, C. W., and Glabe, C. G. (2003) Common structure of soluble amyloid oligomers implies common mechanism of pathogenesis. *Science* **300**, 486-489
28. Fujiwara, H., Hasegawa, M., Dohmae, N., Kawashima, A., Masliah, E., Goldberg, M. S., Shen, J., Takio, K., and Iwatsubo, T. (2002) alpha-Synuclein is phosphorylated in synucleinopathy lesions. *Nat Cell Biol* **4**, 160-164
29. Karpowicz, R. J., Jr., Haney, C. M., Mihaila, T. S., Sandler, R. M., Petersson, E. J., and Lee, V. M. (2017) Selective imaging of internalized proteopathic alpha-synuclein seeds in primary neurons reveals mechanistic insight into transmission of synucleinopathies. *J Biol Chem* **292**, 13482-13497
30. Paumier, K. L., Luk, K. C., Manfredsson, F. P., Kanaan, N. M., Lipton, J. W., Collier, T. J., Steece-Collier, K., Kemp, C. J., Celano, S., Schulz, E., Sandoval, I. M., Fleming, S., Dirr, E., Polinski, N. K., Trojanowski, J. Q., Lee, V. M., and Sortwell, C. E. (2015) Intrastriatal injection of pre-formed mouse alpha-synuclein fibrils into rats triggers alpha-synuclein pathology and bilateral nigrostriatal degeneration. *Neurobiol Dis* **82**, 185-199
31. Rey, N. L., Steiner, J. A., Maroof, N., Luk, K. C., Madaj, Z., Trojanowski, J. Q., Lee, V. M., and Brundin, P. (2016) Widespread transneuronal propagation of alpha-synucleinopathy triggered in olfactory bulb mimics prodromal Parkinson's disease. *The Journal of experimental medicine* **213**, 1759-1778

32. Masuda-Suzukake, M., Nonaka, T., Hosokawa, M., Oikawa, T., Arai, T., Akiyama, H., Mann, D. M., and Hasegawa, M. (2013) Prion-like spreading of pathological alpha-synuclein in brain. *Brain* **136**, 1128-1138
33. Popova, B., Kleinknecht, A., and Braus, G. H. (2015) Posttranslational Modifications and Clearing of alpha-Synuclein Aggregates in Yeast. *Biomolecules* **5**, 617-634
34. Pan, W. X., Mao, T., and Dudman, J. T. (2010) Inputs to the dorsal striatum of the mouse reflect the parallel circuit architecture of the forebrain. *Frontiers in neuroanatomy* **4**, 147
35. Vargas, K. J., Schrod, N., Davis, T., Fernandez-Busnadiego, R., Taguchi, Y. V., Laugks, U., Lucic, V., and Chandra, S. S. (2017) Synucleins Have Multiple Effects on Presynaptic Architecture. *Cell Rep* **18**, 161-173
36. Ogawa, N., Hirose, Y., Ohara, S., Ono, T., and Watanabe, Y. (1985) A simple quantitative bradykinesia test in MPTP-treated mice. *Research communications in chemical pathology and pharmacology* **50**, 435-441
37. Dirr, E. R., Ekhator, O. R., Blackwood, R., Holden, J. G., Masliah, E., Schultheis, P. J., and Fleming, S. M. (2018) Exacerbation of sensorimotor dysfunction in mice deficient in Atp13a2 and overexpressing human wildtype alpha-synuclein. *Behavioural brain research* **343**, 41-49
38. Deas, E., Cremades, N., Angelova, P. R., Ludtmann, M. H., Yao, Z., Chen, S., Horrocks, M. H., Banushi, B., Little, D., Devine, M. J., Gissen, P., Klenerman, D., Dobson, C. M., Wood, N. W., Gandhi, S., and Abramov, A. Y. (2016) Alpha-Synuclein Oligomers Interact with Metal Ions to Induce Oxidative Stress and Neuronal Death in Parkinson's Disease. *Antioxidants & redox signaling* **24**, 376-391
39. Angelova, P. R., Ludtmann, M. H., Horrocks, M. H., Negoda, A., Cremades, N., Klenerman, D., Dobson, C. M., Wood, N. W., Pavlov, E. V., Gandhi, S., and Abramov, A. Y. (2016) Ca2+ is a key factor in alpha-synuclein-induced neurotoxicity. *Journal of cell science* **129**, 1792-1801
40. Gao, X., Carroni, M., Nussbaum-Krammer, C., Mogk, A., Nillegoda, N. B., Szlachcic, A., Guilbride, D. L., Saibil, H. R., Mayer, M. P., and Bukau, B. (2015) Human Hsp70 Disaggregase Reverses Parkinson's-Linked alpha-Synuclein Amyloid Fibrils. *Molecular cell* **59**, 781-793
41. Abeliovich, A., Schmitz, Y., Farinas, I., Choi-Lundberg, D., Ho, W. H., Castillo, P. E., Shinsky, N., Verdugo, J. M., Armanini, M., Ryan, A., Hynes, M., Phillips, H., Sulzer, D., and Rosenthal, A. (2000) Mice lacking alpha-synuclein display functional deficits in the nigrostriatal dopamine system. *Neuron* **25**, 239-252
42. Zharikov, A. D., Cannon, J. R., Tapias, V., Bai, Q., Horowitz, M. P., Shah, V., El Ayadi, A., Hastings, T. G., Greenamyre, J. T., and Burton, E. A. (2015) shRNA targeting alpha-synuclein prevents neurodegeneration in a Parkinson's disease model. *The Journal of clinical investigation* **125**, 2721-2735
43. Weihofen, A., Liu, Y., Arndt, J. W., Huy, C., Quan, C., Smith, B. A., Baeriswyl, J. L., Cavegn, N., Senn, L., Su, L., Marsh, G., Auluck, P. K., Montrasio, F., Nitsch, R. M., Hirst, W. D., Cedarbaum, J. M., Pepinsky, R. B., Grimm, J., and Weinreb, P. H. (2018) Development of an aggregate-selective, human-derived alpha-synuclein antibody BIIB054 that ameliorates disease phenotypes in Parkinson's disease models. *Neurobiol Dis* **124**, 276-288
44. Winner, B., Jappelli, R., Maji, S. K., Desplats, P. A., Boyer, L., Aigner, S., Hetzer, C., Loher, T., Vilar, M., Campioni, S., Tzitzilonis, C., Soragni, A., Jessberger, S., Mira, H., Consiglio, A., Pham, E., Masliah, E., Gage, F. H., and Riek, R. (2011) In vivo demonstration that alpha-synuclein oligomers are toxic. *Proc Natl Acad Sci U S A* **108**, 4194-4199
45. Di Maio, R., Barrett, P. J., Hoffman, E. K., Barrett, C. W., Zharikov, A., Borah, A., Hu, X., McCoy, J., Chu, C. T., Burton, E. A., Hastings, T. G., and Greenamyre, J. T. (2016) alpha-Synuclein binds to TOM20 and inhibits mitochondrial protein import in Parkinson's disease. *Science translational medicine* **8**, 342ra378
46. Mor, D. E., Tsika, E., Mazzulli, J. R., Gould, N. S., Kim, H., Daniels, M. J., Doshi, S., Gupta, P., Grossman, J. L., Tan, V. X., Kalb, R. G., Caldwell, K. A., Caldwell, G. A., Wolfe, J. H., and

Ischiropoulos, H. (2017) Dopamine induces soluble alpha-synuclein oligomers and nigrostriatal degeneration. *Nature neuroscience* **20**, 1560-1568

47. Holmes, B. B., DeVos, S. L., Kfoury, N., Li, M., Jacks, R., Yanamandra, K., Ouidja, M. O., Brodsky, F. M., Marasa, J., Bagchi, D. P., Kotzbauer, P. T., Miller, T. M., Papy-Garcia, D., and Diamond, M. I. (2013) Heparan sulfate proteoglycans mediate internalization and propagation of specific proteopathic seeds. *Proc Natl Acad Sci U S A* **110**, E3138-3147
48. Mao, X., Ou, M. T., Karuppagounder, S. S., Kam, T. I., Yin, X., Xiong, Y., Ge, P., Umanah, G. E., Brahmachari, S., Shin, J. H., Kang, H. C., Zhang, J., Xu, J., Chen, R., Park, H., Andrabi, S. A., Kang, S. U., Goncalves, R. A., Liang, Y., Zhang, S., Qi, C., Lam, S., Keiler, J. A., Tyson, J., Kim, D., Panicker, N., Yun, S. P., Workman, C. J., Vignali, D. A., Dawson, V. L., Ko, H. S., and Dawson, T. M. (2016) Pathological alpha-synuclein transmission initiated by binding lymphocyte-activation gene 3. *Science* **353**
49. Shrivastava, A. N., Redeker, V., Fritz, N., Pieri, L., Almeida, L. G., Spolidoro, M., Liebmann, T., Bousset, L., Renner, M., Lena, C., Aperia, A., Melki, R., and Triller, A. (2015) alpha-synuclein assemblies sequester neuronal alpha3-Na+/K+-ATPase and impair Na+ gradient. *EMBO J* **34**, 2408-2423
50. Luk, K. C., Kehm, V. M., Zhang, B., O'Brien, P., Trojanowski, J. Q., and Lee, V. M. (2012) Intracerebral inoculation of pathological alpha-synuclein initiates a rapidly progressive neurodegenerative alpha-synucleinopathy in mice. *The Journal of experimental medicine* **209**, 975-986
51. Prusiner, S. B., Woerman, A. L., Mordes, D. A., Watts, J. C., Rampersaud, R., Berry, D. B., Patel, S., Oehler, A., Lowe, J. K., Kravitz, S. N., Geschwind, D. H., Glidden, D. V., Halliday, G. M., Middleton, L. T., Gentleman, S. M., Grinberg, L. T., and Giles, K. (2015) Evidence for alpha-synuclein prions causing multiple system atrophy in humans with parkinsonism. *Proc Natl Acad Sci U S A* **112**, E5308-5317
52. Peng, C., Gathagan, R. J., Covell, D. J., Medellin, C., Stieber, A., Robinson, J. L., Zhang, B., Pitkin, R. M., Olufemi, M. F., Luk, K. C., Trojanowski, J. Q., and Lee, V. M. (2018) Cellular milieu imparts distinct pathological alpha-synuclein strains in alpha-synucleinopathies. *Nature* **557**, 558-563
53. Volpicelli-Daley, L. A., Luk, K. C., and Lee, V. M. (2014) Addition of exogenous alpha-synuclein preformed fibrils to primary neuronal cultures to seed recruitment of endogenous alpha-synuclein to Lewy body and Lewy neurite-like aggregates. *Nat Protoc* **9**, 2135-2146
54. Laue, T. M., Shaw, B. D., and Ridgeway, S. M. (1992) Computer-aided interpretation of analytical sedimentation data for proteins. *Analytical Ultracentrifugation in Biochemistry and Polymer Science*, 90-125
55. Volpicelli-Daley, L. A., and Levey, A. (2004) Immunohistochemical localization of proteins in the nervous system. *Current protocols in neuroscience* **Chapter 1**, Unit 1 2
56. Rutherford, N. J., Brooks, M., and Giasson, B. I. (2016) Novel antibodies to phosphorylated alpha-synuclein serine 129 and NFL serine 473 demonstrate the close molecular homology of these epitopes. *Acta neuropathologica communications* **4**, 80
57. Hersch, S. M., Yi, H., Heilman, C. J., Edwards, R. H., and Levey, A. I. (1997) Subcellular localization and molecular topology of the dopamine transporter in the striatum and substantia nigra. *The Journal of comparative neurology* **388**, 211-227

FOOTNOTES

Funding support for this project was provided by the Michael J Fox Foundation to L.V.-D and N.C. Support from the Cambridge Centre for Misfolding Disease is acknowledged by M.C.-C., J.R.K., and C.M.D.

The abbreviations used are: analytical ultracentrifugation (AUC), atomic force microscopy (AFM), circular dichroism (CD), Fourier transform infrared (FTIR), paraformaldehyde (PFA), phosphate buffered saline (PBS), Thioflavin T (ThioT), transmission electron microscopy (TEM)

Species	Average length (nm)	Secondary Structure	Configuration	Amyloid	Seeding competent
Monomer	N/A	Random coil	N/A	No	No
Fibrils	266	60% β-sheet	Parallel	Yes	Yes
Fragmented fibrils (mix, "F-M")	120	60% β-sheet	Parallel	Yes	Yes
Fragmented fibrils (short, "F-S")	70	60% β-sheet	Parallel	Yes	Yes
Oligomers ("O")	54	30% β-sheet	Anti-Parallel	No	No

Table 1. Summary of biophysical characteristics of the species of α-synuclein used in this study.

Brain area	Average p-α-synuclein score-ipsilateral	Average p-α-synuclein score-contralateral
Motor Cortex	1.6	1.1
Somatosensory Cortex	1.6	1
Insular Cortex	1.6	1
SNc	1.6	0
Auditory Cortex	1.4	0.9
Lateral Orbital Cortex	1.3	0.9
Amygdala	1.3	0.6
Ectorhinal Cortex	1.3	0.9
Striatum	1.1	0.5
Cingulate Cortex	1.0	1.0
Visual Cortex	1.0	0.4
Piriform Cortex	1.0	0.5
Nucleus Accumbens	0.4	0.4
Retrosplenal Cortex	0.7	0.3
Subiculum	.6	0
Hippocampus	0.4	0
Mammillary nucleus	0.5	0.1
Olfactory Tubercle	0.2	0
Fimbria	0	0
Cerebellar Flocculus	0	0
Colliculus	0	0

Table 2. Mice received unilateral striatal injections of F-S and were perfused three months later. Immunohistochemistry was performed on brain sections using an antibody to p-α-synuclein. The abundance of inclusions in these brain areas was rated on a scale from 0 to 3 (see Supplementary material 1) and the brain areas are listed in order of average score. Brains from nine independent mice were scored to obtain the average score.

Figures

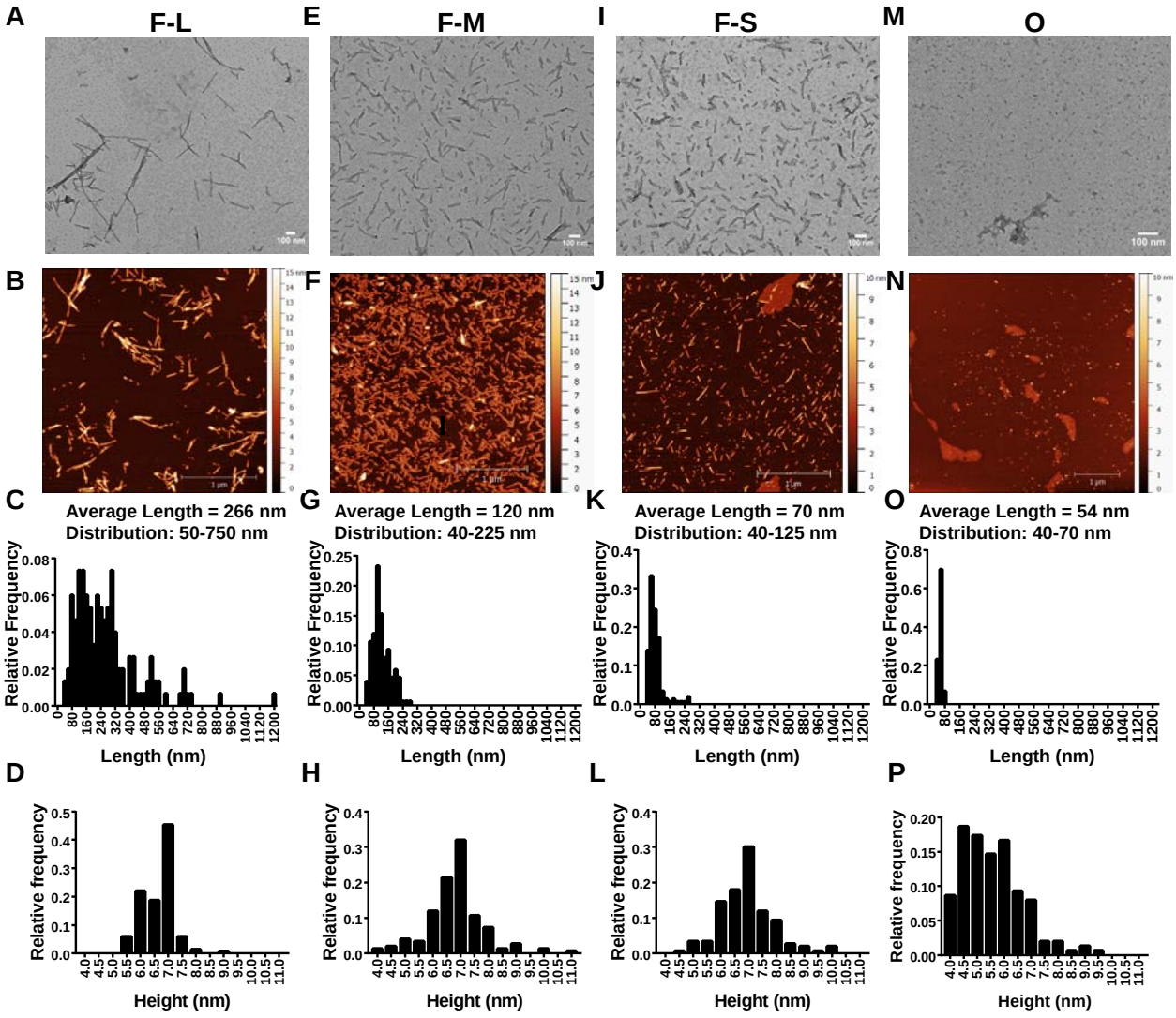

Figure 1. Morphological characterization of the mouse α-synuclein species used in the *in vivo* mouse studies. TEM and AFM images of fibrils (F-L) (A,B), sonicated fibrils (F-M) (E,F), sonicated fibrils enriched in short fragments (F-S) (I,J), and oligomers (O) (M,N). (C-P).AFM was used to quantify the length and height of each species shown in the histograms.

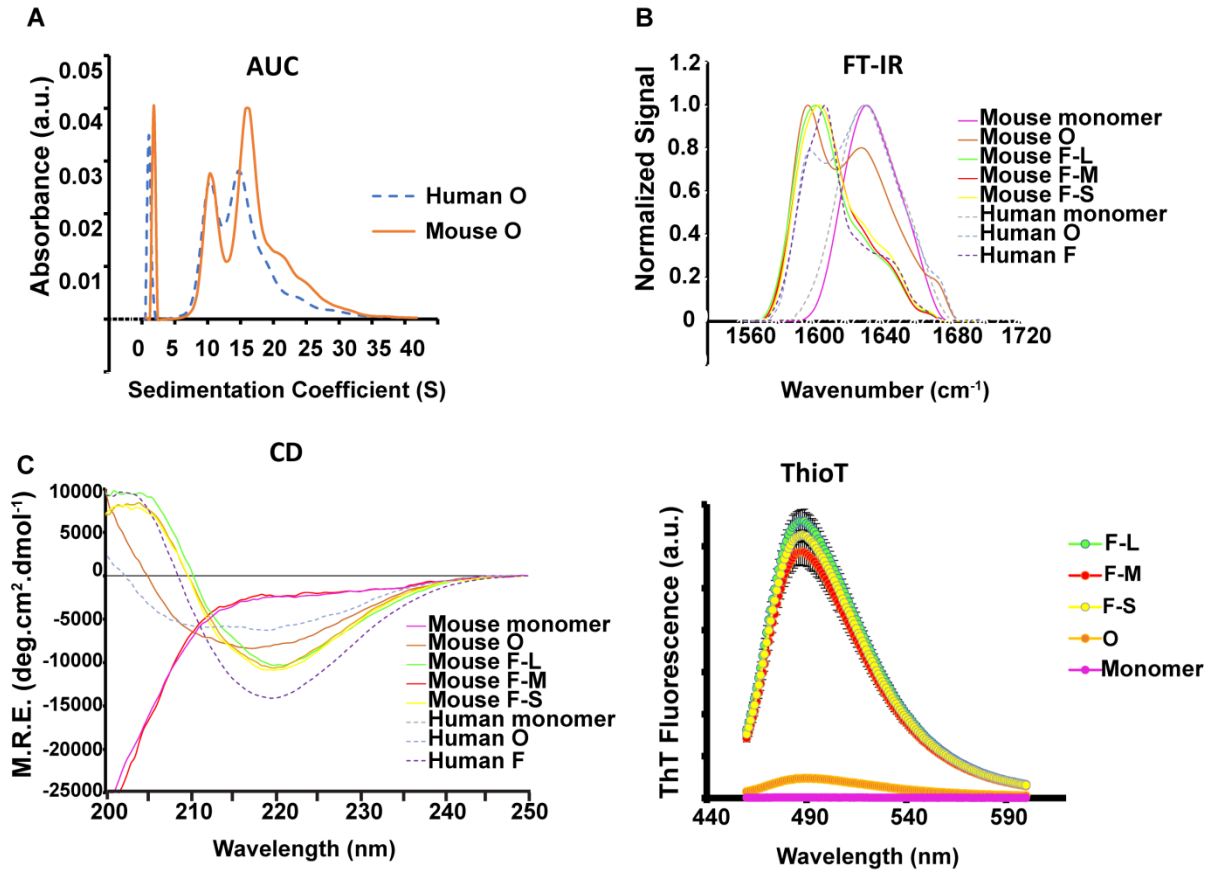

Figure 2. Structural characterization of α-synuclein species used in the *in vivo* mouse studies. (A) AU sedimentation velocity measurement of human (blue dashed line) and mouse oligomers (orange line) shows 10S and 15S species. (B) FTIR spectra shows that F-L, F-M, and F-S species are primarily composed of parallel β-sheet (band at 1,620-1630), and that the oligomeric (mouse and human) species are primarily antiparallel (band at 1620-1630 cm^{-1} and shoulder at 1695cm^{-1}). The mouse and human oligomers have β-sheet structure of about 40% and 65%, respectively. (C) CD show that β-sheet content of oligomers (mouse and human) are intermediate between monomer and fibrils. (D) ThioT binding shows that the fibrils adopt an amyloid conformation, the oligomers show limited ThioT binding and monomer shows no ThioT binding.

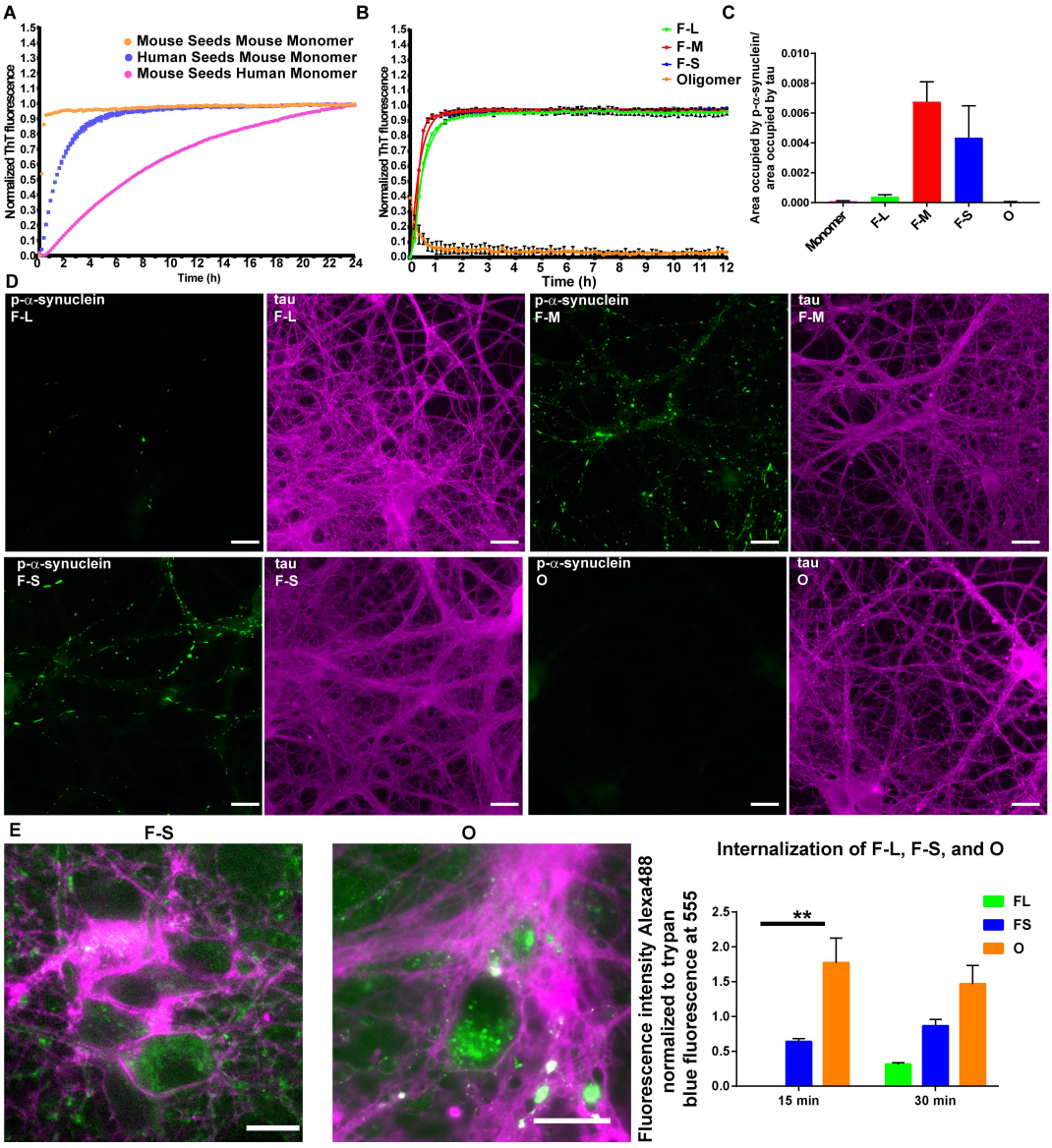

Figure 3. Seeding ability of the difference assembled forms of α-synuclein species *in vitro* and in primary neurons. (A,B) Monomer (100 μM) was incubated with 5 μM fibrillar or oligomeric seeds and the fluorescence of samples incubated with ThioT was quantified over time. (C,D) For the primary hippocampal neurons, 70 nM of F-L, F-M, F-S or oligomers were added to the neurons and after seven days, the neurons were fixed and inclusion formation was visualized using an antibody to p-α-synuclein (green). Immunofluorescence for tau (magenta) shows the distribution of axons (Scale bar = 50 μM). Image J was used to quantify the percent area occupied by p-α-synuclein fluorescence normalized to the area occupied by tau fluorescence. The data are presented as the mean ± SEM. (E) Primary hippocampal neurons were pre-incubated with Alexa 488 tagged F-L, F-S or O for 30 min at 4°C to allow binding to the cell surface. The neurons were then incubated for 15 or 30 min at 37ºC to allow internalization. Fluorescence of external α-synuclein-Alexa 488 was quenched using trypan blue. Images show representative α-synuclein-Alexa 488 fibrils or oligomers. When trypan blue binds to proteins on the cell surface it fluoresces at 560 nm which is shown in the images as magenta (Scale bar = 50 μM). The fluorescence intensity of Alexa 488 from 10 fields per condition was quantified and normalized to trypan blue immunofluorescence. The internalization experiments were repeated two times.

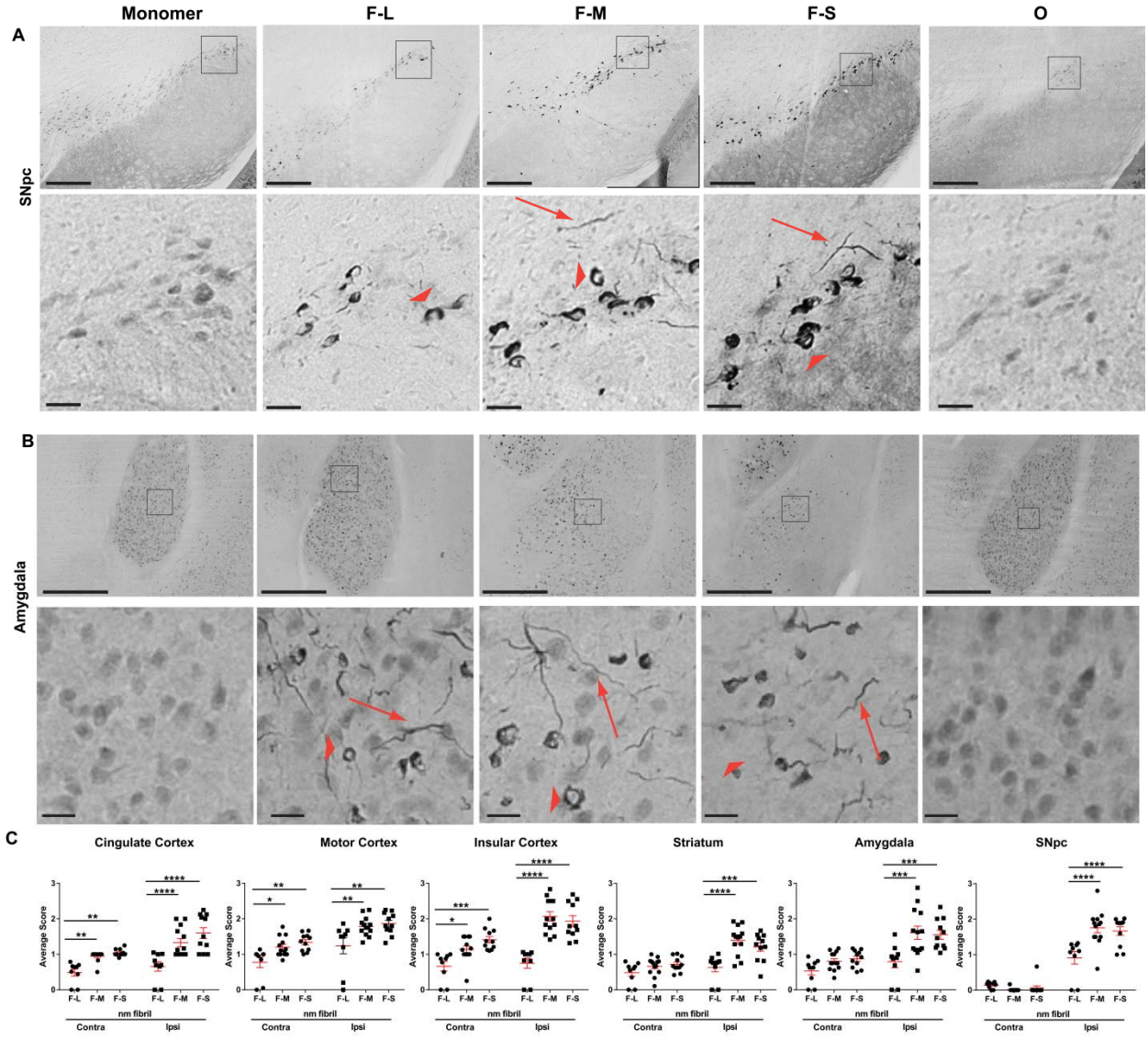

Figure 4. Inclusion formation in the mouse brain after injection of different forms of α-synuclein. C57BL/6J mice received unilateral striatal injections of two µL of soluble monomer (300 µM), F-L (150 µM), F-M (150 µM), F-S (150 µM) and O (300 µM). After three months, mice were perfused and immunohistochemistry was performed using an antibody to p-α-synuclein. Representative images from the SNc (A) and amygdala (B) are shown. Arrowheads indicate inclusions in the soma and arrows indicate Lewy neurite-like inclusions. (C) The abundance of inclusions were measured by an investigator blinded to experimental conditions (Supporting Material 1). Numbers of mice: monomer (12), F-L (11), F-M (12), F-S (11), O (15). Data are shown as the mean score ± SEM and were analyzed using a two-way ANOVA, α-synuclein species/cingulate $F(2,30) = 37.85$, $p < 0.0001$; α-synuclein species/motor cortex $F(2,30) = 7.9$, $p < 0.002$; α-synuclein species/insular cortex $F(2,30) = 22.3$, $p < 0.0001$; α-synuclein species/striatum $F(2,30) = 8.5$, $p < 0.001$; α-synuclein species/amygdala $F(2,30) = 6.6$, $p = 0.004$; α-synuclein species/SNc $F(2,30) = 6.2$, $p < 0.005$. *p<0.05, **p<0.01, ***p<0.001, ****p<0.0001. Scale bar = 100 µm (top panels); 20 µm (bottom panels).

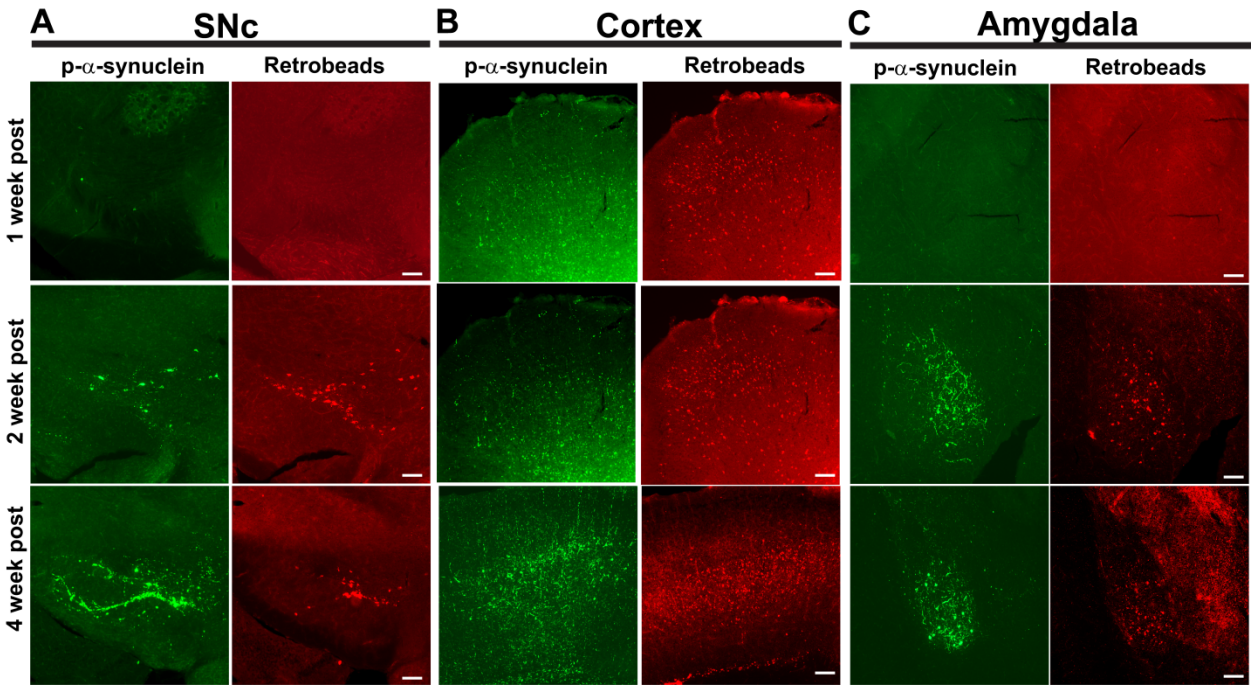

Figure 5. Appearance of p-α-synuclein inclusions in brain areas that project to the striatum. Fibrils and retrotracer beads were co-injected unilaterally into the striatum. After, one (N=3), two (N=3) or 4 weeks (N=3), mice were perfused and immunofluorescence to p-α-synuclein (green) was performed. The retrotracer beads are shown in red and the merged images include p-α-synuclein, retrotracer beads and Hoeschst (blue). Representative images from the SNc, motor cortex and amygdala are shown.

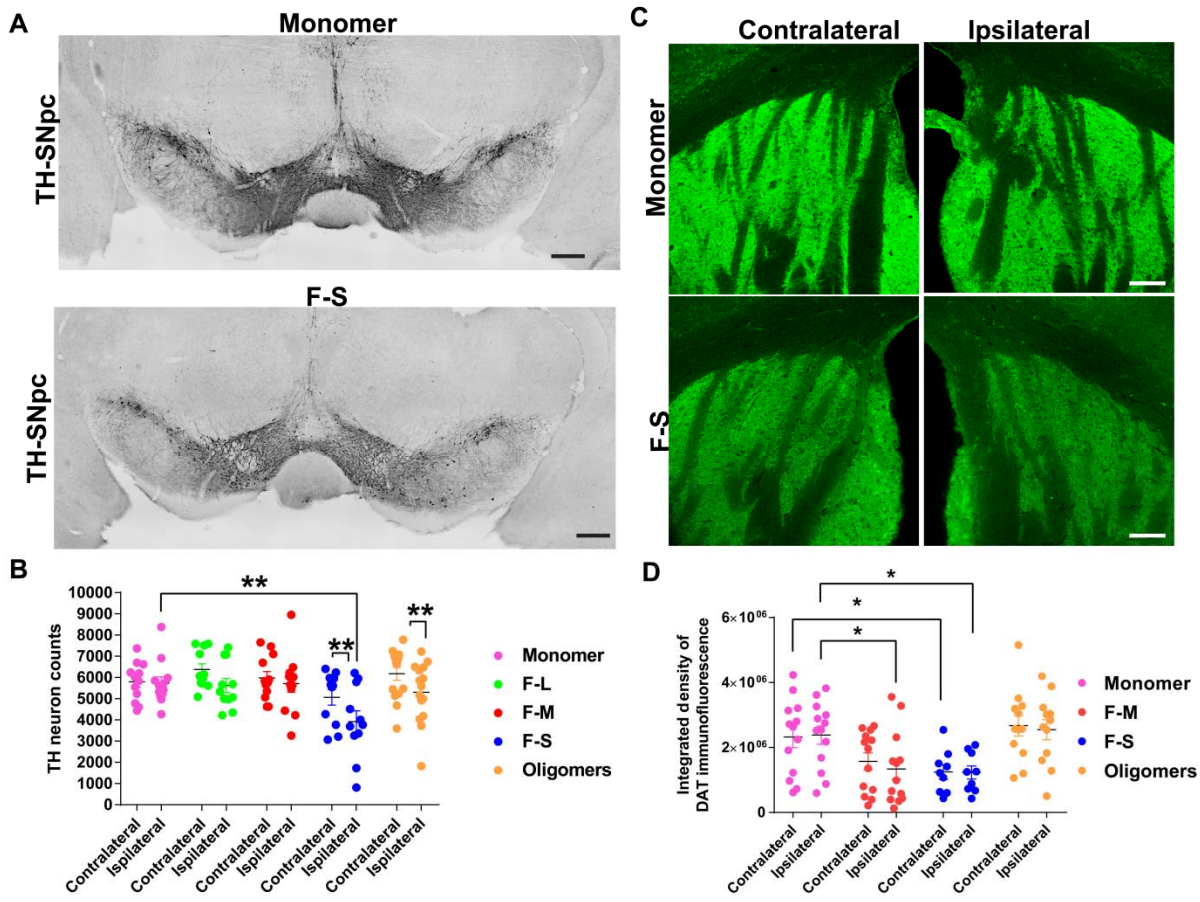

Figure 6. Quantitation of TH-positive neurons in the SNc, and DAT terminals in striatum following unilateral striatal injections of different α-synuclein species. C57BL/6J mice received unilateral striatal injections of two µL of soluble monomer (300 µM), F-L (150 µM), F-M (150 µM), F-S (150 µM) and O (300 µM). After three months, the mice were perfused and immunostaining was performed. Numbers of mice: monomer (12), F-L (11), F-M (12), F-S (11), O (15) (A) Representative images of tyrosine hydroxylase immunohistochemistry in the SNc of monomer and F-S injected mice. (B) Unbiased stereology of tyrosine hydroxylase positive neurons performed by an investigator blinded to experimental conditions. Data are shown as the mean counts ± SEM and analyzed using a two-way ANOVA, α-synuclein species $F(5,67) = 2.7$, $p = 0.03$. (C) Immunofluorescence performed using antibodies for both DAT and an Alexa-488-goat anti-rat secondary (shown above), and TH and an Alexa-555-goat anti-chicken secondary. Images were captured using confocal microscopy. Representative images of DAT in the striatum from monomer and F-S injected mice are shown. See also Supplemental Figure 5 which shows TH immunofluorescence from the same monomer striatal section shown in this figure, and quantitation of TH in the striatum. (D) Image J was used to quantify the integrated fluorescence intensity of DAT in the striatum. Data are shown as the mean counts ± SEM and analyzed using a two-way ANOVA, α-synuclein species $F(3,43) = 5.7$, $p = 0.002$. *p<0.05, **p<0.01, ***p<0.001, ****p<0.0001. Scale bar = 100 µm.

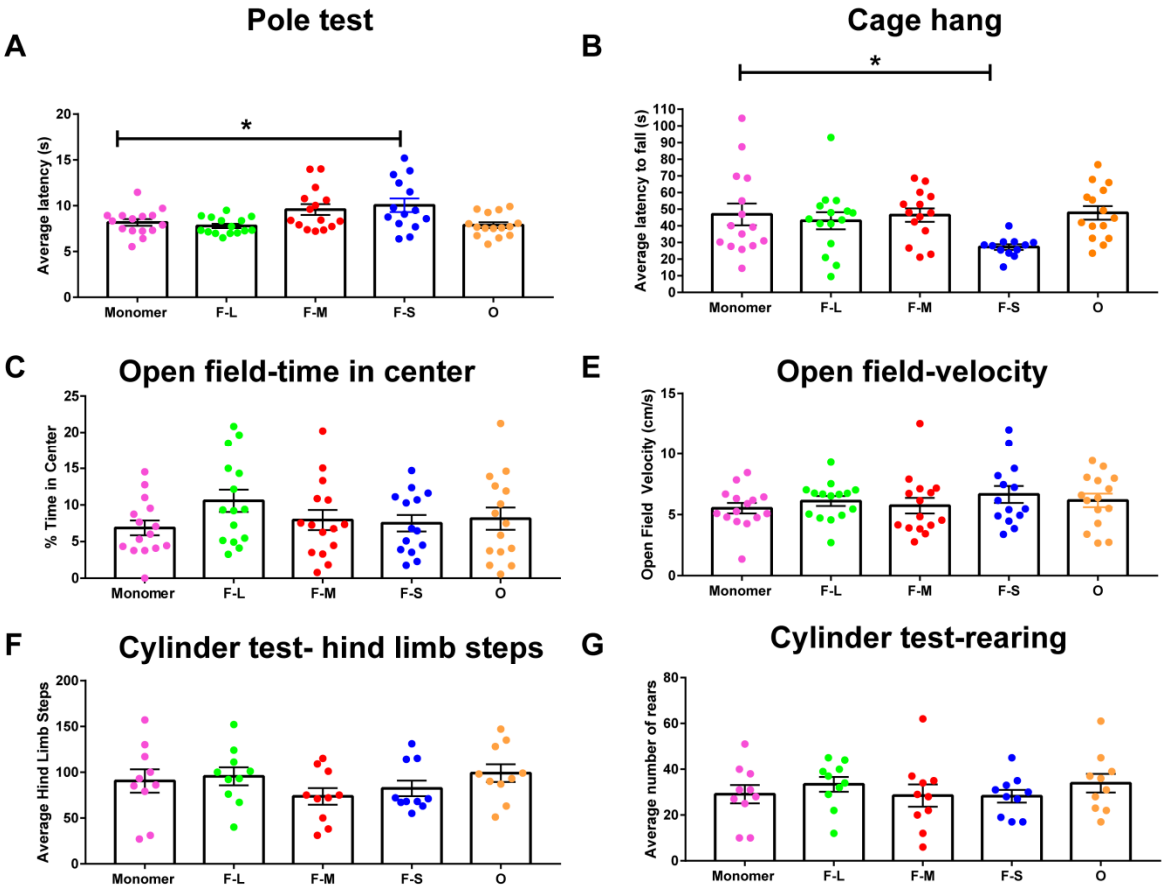

Figure 7. Motor behavior of mice following unilateral striatal injections of different α-synuclein species. C57BL/6J mice received unilateral striatal injections of two µL of monomer (300 µM), F-L (150 µM), F-M (150 µM), F-S (150 µM) and O (300 µM). Three months later, mice were subjected to the following behavior tests: open field, pole test, cage hang, cylinder test (modified for mice). Numbers of mice for pole test, cage hang, open field: monomer (12), F-L (11), F-M (12), F-S (11), O (15). Numbers of mice for cylinder test: monomer (10), F-L (10), F-M (10), F-S (10), O (10). The data were analyzed by one-way ANOVA: pole test $F(4,69) = 4.7$, $p = 0.002$; cage hang $F(4,66) = 2.86$, $p = 0.03$; open field/%time center $F(4,69) = 1,1$, $p = NS$; open field/velocity $F(4,69) = 0.6$, $p = NS$; hind limb steps $F(4,45) = 1.1$, $p = NS$; rearing $F(4,45) = 0.5$, $p = NS$.

Defining α-synuclein species responsible for Parkinson disease phenotypes in mice

Jessica M. Froula, Marta Castellana-Cruz, Nadia M. Anabtawi, José D. Camino, Serene W. Chen, Drake R. Thrasher, Jennifer Freire, Allen A. Yazdi, Sheila Fleming, Christopher M. Dobson, Janet R. Kumita, Nunilo Cremades and Laura A. Volpicelli-Daley

J. Biol. Chem. published online May 29, 2019

Access the most updated version of this article at doi: 10.1074/jbc.RA119.007743